J. Fluid Mech. (1992), *vol.* 243, *pp.* 541–560
Printed in Great Britain

An investigation of wall-layer dynamics using a combined temporal filtering and correlation technique

By A. M. NAGUIB AND C. E. WARK

Illinois Institute of Technology, Fluid Dynamics Research Center, Department of Mechanical and Aerospace Engineering, Chicago, IL 60616, USA

(Received 9 August 1991 and in revised form 6 March 1992)

The relative role of outer- and wall-layer structures in the dynamics of the near-wall region of a turbulent boundary layer was explored by examining the scaling of the spanwise correlation coefficient between the wall shear stress and the streamwise velocity fluctuation, $R_{\tau u}(z)$, within narrow frequency bands spanning the entire turbulence spectrum. The scaling characteristics of $R_{\tau u}(z)$ within the individual frequency bands indicate that one can separate the contribution to the streamwise velocity fluctuations, in the buffer and logarithmic regions, due to outer-layer structures from those due to wall-layer events. Results provide insight into the lack of wall scaling for the conventional correlation coefficient, $R_{\tau u}(z)$, in the near-wall region. Moreover, the 'negative dip' in $R_{\tau u}(z^+)$, which has often been associated with the low-speed streaks, was found to exist within certain frequency bands for all Reynolds numbers investigated ($1579 \leqslant Re_\theta \leqslant 5961$). More interestingly, it is shown that, although the energy of the outer-layer structures increases with Reynolds number to overwhelm the streamwise velocity fluctuations in the near-wall region, the production of the Reynolds shear stress is dominated by wall-layer eddies. The findings of the current investigation provide strong support for Townsend's hypothesis of 'active' and 'inactive' motions.

1. Introduction

1.1. *Background*

Understanding the dynamics of turbulent boundary layers remains an unyielding problem in today's fluid dynamics research. During the past three decades the main focus of boundary-layer research has been the identification of organized, repeatable motions (coherent structures) and their role in the generation and sustaining of turbulence: for a comprehensive review see Robinson (1991*a*, *b*). This type of research resulted in the discovery of a variety of structures with a wide range of scales spanning the gap between the viscous lengthscale (ν/u_τ) and the boundary-layer thickness (δ). Today there is considerable controversy regarding the existence of, the dynamical significance of and the interaction between the different structures: indeed, there seem to be more questions than answers in boundary-layer research.

One of the fundamental approaches in the study of turbulent boundary layers is to investigate the scaling of turbulent quantities. In this approach the issue is which of the two competing scales in the boundary layer, i.e. inner (kinematic viscosity ν, and wall-friction velocity u_τ) and outer (boundary-layer thickness δ, and free-stream velocity U_∞), renders a given turbulent quantity independent of Reynolds-number

variations. Successful scaling of a turbulent quantity with either wall (inner) or outer scales implies that the dynamics of the turbulent motion(s) producing the turbulent quantity is controlled by either the wall layer or the outer region of the boundary layer respectively. The drawbacks of the scaling approach are that, most of the time, it does not distinguish amongst contributions from different classes of structures and it does not provide a kinematical description of the turbulent motions involved. However, the approach provides a powerful tool to investigate boundary-layer dynamics while avoiding the subjectiveness and controversy involved in defining coherent structures.

The mean velocity profile has one of the few well-established scaling characteristics in turbulent boundary layers, where wall variables are the appropriate scales near the wall, outer scales are successful away from the wall and both inner and outer scales are appropriate in the intermediate (logarithmic) region. Detailed reviews for the scaling of the mean velocity profile are given by Clauser (1956) and Laufer (1950). The streamwise turbulent kinetic energy, $\overline{u^2}$, scales with wall variables very close to the wall and with outer variables away from the wall. However, in the logarithmic region, both inner and outer variables fail to collapse $\overline{u^2}$ profiles (e.g. Blackwelder & Haritonidis 1983 and McLean 1990). For a long time, researchers have assumed that the turbulent stresses scale with wall variables in the near-wall region; however, this conventional wisdom was challenged by high-resolution-LDV measurements of the streamwise, u, and normal, v, velocity components by Wei & Willmarth (1989) in turbulent channel flow. These LDV measurements, over the Reynolds-number range (based on channel half-width and centreline velocity) 3000–40000, showed that $\overline{u^2}$ scales with wall variables only up to $y^+ \approx 12$, while the normal, $\overline{v^2}$, and shear, $\overline{uv}$, Reynolds stresses do not scale with wall variables at any height in the boundary layer.

To gain a better understanding of the scaling of the dominant turbulent eddies in the boundary layer, McLean (1990) investigated the scaling of the spanwise two-point correlation coefficient, $R_{uu}(z)$, for the Reynolds number range $1500 \leqslant Re_\theta \leqslant 10290$. The correlation data were obtained at several normal, y, positions such that the non-dimensional heights, $y^+ = yu_\tau/\nu$ and y/δ, were matched among the different Reynolds numbers. McLean (1990) concluded that except for small spanwise offsets in the near-wall region, $R_{uu}(z)$ scaled with outer variables throughout the boundary layer: data were taken as close to the wall as $y^+ = 15$. A similar investigation was carried out by Wark, Robinson & Naguib (1991), who examined the scaling of the spanwise correlation coefficient between the wall shear stress, τ, and the streamwise velocity, u, for both experimental results ($1579 \leqslant Re_\theta \leqslant 5961$) and Spalart's (1988) direct numerical simulation results for a turbulent boundary layer at $Re_\theta = 670$ and 1410. In their investigation, Wark *et al.* (1991) took measurements as close to the wall as $y^+ = 10$ and used a set of fine-increment spanwise offsets, Δz. The scaling of $R_{\tau u}(z)$ showed a 'dual' character within the buffer region, where wall variables collapsed the correlation curves for small spanwise offsets at fixed y^+ positions while outer variables collapsed the correlation curves for large spanwise offsets at fixed y/θ positions. In the logarithmic region, $R_{\tau u}(z)$ scaled with outer variables over the entire range of spanwise offsets.

Generally, most of the emphasis in boundary-layer research has been placed on the near-wall region where most of the Reynolds stress and turbulent kinetic energy production takes place. However, the failure of turbulent quantities to scale on inner variables in the near-wall region leads investigators to believe that the outer-layer structures play a role in wall-layer dynamics, i.e. there is inner–outer interaction.

The existence of large-scale structures whose effect is felt simultaneously in the near-wall and outer regions has been documented through the correlation measurements from Brown & Thomas (1977), the simultaneous rack probe measurement from Chen & Blackwelder (1987), the conditionally averaged structures from Wark & Nagib (1991), and others. Although the large-scale turbulent motions leave their imprint on the wall, the question is still open of whether they affect the dynamics of the flow, leading to the generation of the turbulent shear stress and kinetic energy in the near-wall region, or their effect near the wall is merely an 'inactive' motion as hypothesized by Townsend (1961) and further investigated by Bradshaw (1967).

1.2. *Objectives*

The existence of turbulent motions that scale with wall variables in the near-wall region is more than just an intuitive idea; for example, the prominent wall-layer streaky structure is known to scale with wall variables (Smith & Metzler 1983). In the present paper, the scaling of the spanwise correlation coefficient $R_{\tau u}(z)$ will be further explored in order to understand the lack of wall scaling in the near-wall region. Rather than calculating the conventional correlation which arises due to an indiscriminant integral effect of different types of structures, the correlation coefficient $R_{\tau u}(z)$ will be determined for narrow-band-passed τ (measured at the wall) and u (measured at different y-positions in the buffer and logarithmic regions) signals and their scaling will be examined. If $R_{\tau u}(z)$ for the temporally filtered signals scale with either wall or outer variables then the dynamics of the turbulent motion(s) within the passed frequency band is, presumably, solely controlled by the wall region or outer layer respectively. If successful, the approach will provide a means of isolating the contribution of outer-layer structures to the turbulent fluctuations from those due to wall-layer structures. Finally, an attempt will be made to assess the contribution and relative importance of outer- and inner-layer structures to the dynamics of turbulence in the near-wall region.

2. Data acquisition and analysis

2.1. *Experimental set-up*

Experiments were carried out in the Mark V. Morkovin low-turbulence-intensity closed-return wind tunnel at IIT. The turbulent boundary layer develops along a mirror-finish aluminium flat plate which is located in the 91 cm high × 61 cm wide × 6 m long test section, downstream of a 4:1 contraction. The flat plate is positioned 30 cm above the test section floor, leaving a 61 cm × 61 cm flow area on top of the plate. Transition to turbulence is triggered using a flush-mounted sandpaper strip, located about 20 cm downstream of the leading edge of the flat plate. A movable ceiling is adjusted to attain a zero streamwise pressure gradient in the test section.

The same data set as that reported by Wark *et al.* (1991) was used for the current investigation: a brief description follows. Six different Reynolds numbers covering the range, $1579 \leqslant Re_\theta \leqslant 5961$, were attained by changing the free-stream velocity (U_∞) while maintaining the same streamwise (x) measurement location. The Reynolds numbers and the corresponding relevant boundary-layer parameters can be found in table 1.

Hot-wire probes were used to measure the fluctuating wall shear stress (τ) and the fluctuating streamwise velocity (u) simultaneously. The wall-shear probe was made up of a Plexiglas plug whose surface is coated with Ardyl (a material having a low

U_∞ (m/s)	u_τ (m/s)	θ (cm)	Re_θ	l^+
4.5	0.20	0.53	1579	6.5
5.3	0.23	0.59	2050	7.5
6.7	0.27	0.65	2841	8.8
9.9	0.38	0.65	4155	12.4
11.8	0.44	0.64	4939	14.3
14.6	0.53	0.63	5961	17.2

TABLE 1. Boundary-layer parameters

thermal conductivity) on top of which a hot wire is placed and soldered to two prongs that pass through the plug. A conventional static calibration procedure was used to calibrate the wall-shear probe. The calibration velocity was taken as the friction velocity (u_τ), which was known *a priori* using a Clauser fit to a set of mean velocity profiles which were acquired at a number of wind tunnel velocities covering a sufficiently wide range. In a detailed study of wall-shear-stress measurements, Alfredsson *et al.* (1988) showed that a static calibration procedure for a probe similar to the one used in the current investigation was adequate for dynamic measurements. The streamwise velocity was measured using a single-wire probe. The hot wires used for measurements of both τ and u were 2.5 μm in diameter and were copper plated leaving a sensing length, $l = 0.5$ mm (l^+ ($= lu_\tau/\nu$) values are given in table 1).

The single-wire probe was used to measure u in a two-dimensional measurement grid. The measurement positions were chosen such that $y^+ = 10$, 15, 28, 50 and 100 and $y/\theta = 0.078$, 0.265 and 0.445 were matched for the boundary layers at different Reynolds numbers. The spanwise spacing between successive grid locations (Δz) was 0.38 mm ($\Delta z^+ = 5$–13) for the first five positions, 0.5 mm ($\Delta z^+ = 6.5$–17) for the intermediate seven positions, and 1.02 mm ($\Delta z^+ = 13.5$–35) for the last five positions. Spanwise and normal probe movements were achieved using a computer-controlled two-dimensional traversing mechanism. All data were digitized and long time series of 204800 data points per probe were acquired at each location at a non-dimensional digitization increment of $\Delta t^+ = 2$.

2.2. *Data processing*

Prior to calculating $R_{\tau u}(z)$, the acquired τ- and u-signals were digitally band-pass filtered. Since there was no *a priori* knowledge of what cutoff frequencies to choose for the different filters, the entire spectrum of the turbulent fluctuations was systematically divided using 10 equal-width band-pass filters, in addition to a single low-pass filter. The filters used were zero-phase FIR digital filters, designed using a program by McClellan, Parks & Rabiner (1979). Filtering of turbulent signals was achieved by taking the FFT of both the turbulent signal and the impulse response of the filter, followed by multiplying the two transforms in the frequency domain (using the overlap-add method for long time series), and finally taking the inverse FFT of the multiplied signal. Figures 1(*a*) and 1(*b*) show an example of the normalized power spectral density for the non-filtered turbulent signal (solid line) and for the same turbulent signal when filtered using each of the 11 filters (numbered $0, 1, 2, \ldots, 10$) on semi-log and log-log coordinates respectively. Note that the cutoff frequencies for the different filters are scaled on wall variables. A sample turbulent time series before and after filtering, using filters 0, 1 and 2 (which contain about 85% of the energy in the time series), is shown in figure 2. It can be seen from the

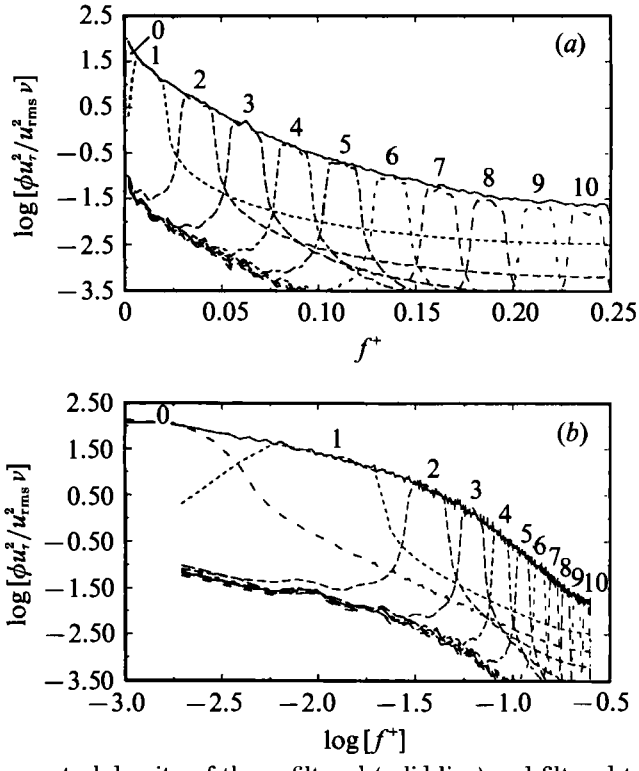

FIGURE 1. Power spectral density of the unfiltered (solid line) and filtered turbulent signal (for 11 different filters) plotted on: (*a*) semi-log and (*b*) log-log coordinates.

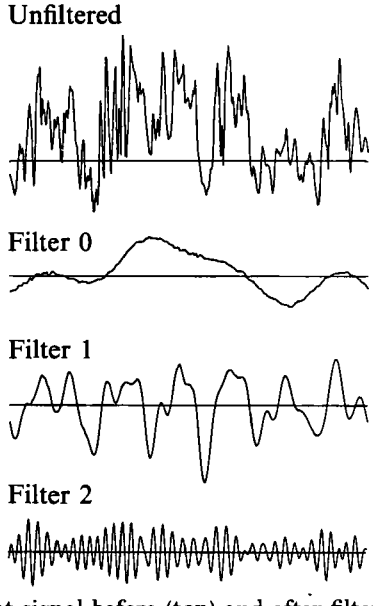

FIGURE 2. A sample turbulent signal before (top) and after filtering (using filters 0, 1 and 2).

figure that the filtered time series follow the original turbulent signal, in the appropriate frequency band.

The spanwise correlation coefficient of the filtered signals was calculated using the equation

$$R_{\tau u}(x=0,y,z,t=0)=\frac{\frac{1}{N}\sum_{i=1}^{N}\tau(x_0,0,0,t_i)\,u(x_0,y,z,t_i)}{\tau_{\rm rms}\,u_{\rm rms}},$$

where τ is the filtered fluctuating streamwise wall shear stress, u is the filtered fluctuating streamwise velocity, x, y and z are the steamwise, normal and spanwise offsets between the wall-shear and velocity probes, and t is the time delay between the τ- and u-signals. The subscript rms denotes the standard deviation of the filtered fluctuating quantity and N is the total number of data points in the time series ($N = 204\,800$).

3. Results

3.1. *Scaling of the spanwise correlations*

The scaling of the conventional correlation coefficient $R_{\tau u}(z)$ in the buffer layer is demonstrated by figure 3 (taken from Wark *et al.* 1991). The figure shows the dependence of $R_{\tau u}$ on the spanwise separation between the single-wire and wall-shear probes for a set of experimental and Spalart's (1988) direct numerical simulation (DNS) results. In figure 3(*a*), one can see that for $y^+ = 10$, $R_{\tau u}(z)$ scales fairly well with wall variables for $z^+ \leqslant 40$ while for $y/\theta = 0.078$ (figure 3*b*), careful inspection reveals that for the highest three Reynolds numbers outer variables collapse $R_{\tau u}(z)$ for $z/\theta \geqslant 0.5$. It is also interesting to note that the prominent negative peak of the spanwise correlation coefficeint at $z^+ \approx 50$ (e.g. see Kreplin & Eckelmann 1979), which has been known to correspond to one-half the average spanwise spacing of the low-speed streaks, cannot be seen in any of the results shown in figure 3. These intriguing characteristics of $R_{\tau u}(z)$ and its scaling in the near-wall region motivated the filtered time-series analysis, the results of which are presented below.

Filters 0, 1 and 2 contain about 85% of the energy in the streamwise velocity fluctuation and, hence, for the remainder of the paper, discussion will mainly focus on these filters. In addition, to facilitate presenting the results, the spanwise correlation coefficient obtained when using filter n will be denoted by ${}_nR_{\tau u}(z)$. Results for the correlation coefficient obtained in the buffer layer using filter 0 are shown in figures 4 and 5: figure 4 shows ${}_0R_{\tau u}(z^+)$ obtained at fixed y^+ values (10, 15 and 28), while figure 5 depicts ${}_0R_{\tau u}(z/\theta)$ when matching $y/\theta = 0.078$ (corresponding y^+ range: 5.5–17.8). It is clear from the figure that when scaled with inner variables, the correlation results experience a strong Reynolds-number dependence, where higher Reynolds numbers result in larger correlation coefficients. Alternatively, when scaled with outer variables (figure 5), ${}_0R_{\tau u}(z/\theta)$ is less sensitive to the change in Reynolds number.

Since ${}_0R_{\tau u}(z)$ results scale better with the outer lengthscale, it would be more appropriate to use filters with cutoff frequencies that match when scaled with outer variables. To arrive at the appropriate cutoff frequency in outer variables, consider the power spectral density (p.s.d.) results shown in figure 6(*a*) for $y/\theta = 0.078$. In the figure, the p.s.d. for six different Reynolds numbers is normalized such that the area under the semi-log plot is $u^2_{\rm rms}/U^2_\infty$. In the frequency range $\log(f^\circ) \leqslant -2.00$ (or

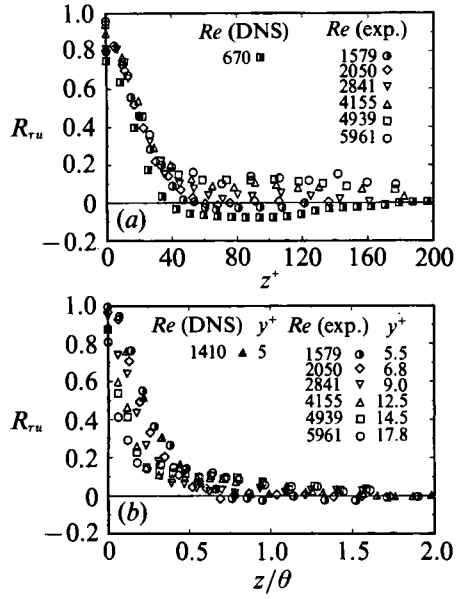

FIGURE 3. (*a*) Inner ($y^+ = 10$) and (*b*) outer ($y/\theta = 0.078$) scaling characteristics of the conventional spanwise correlation coefficient in the buffer region.

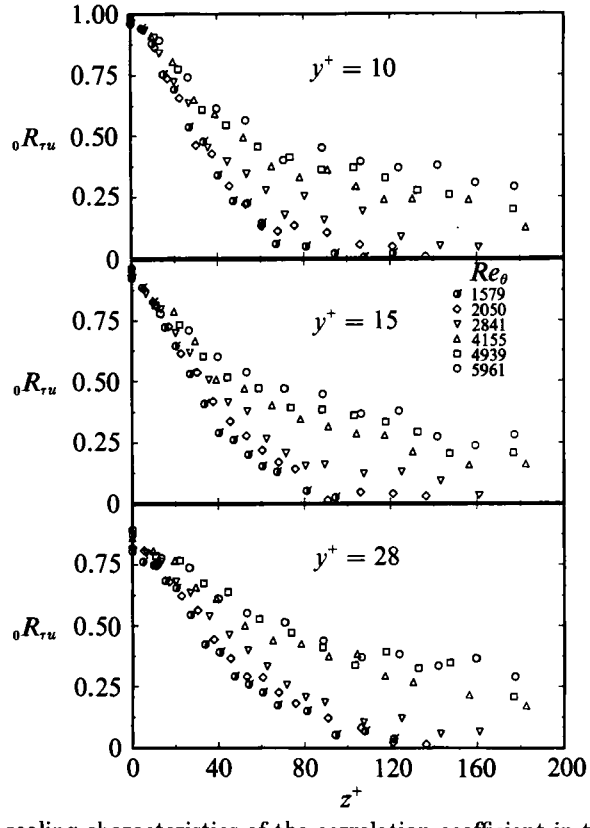

FIGURE 4. Inner scaling characteristics of the correlation coefficient in the buffer region ($y^+ = 10$, 15 and 28) for the filtered time series, using filter 0.

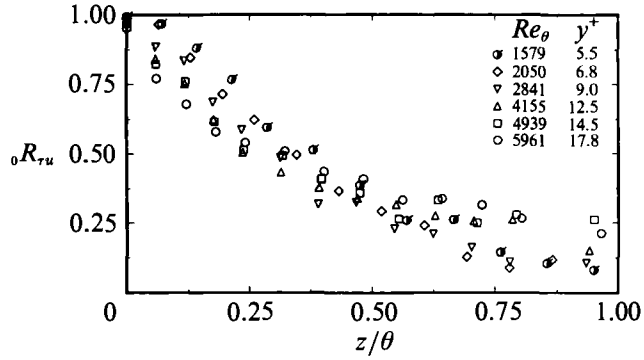

FIGURE 5. Outer scaling characteristics of the correlation coefficient in the buffer region ($y/\theta = 0.078$) for the filtered time-series, using filter 0.

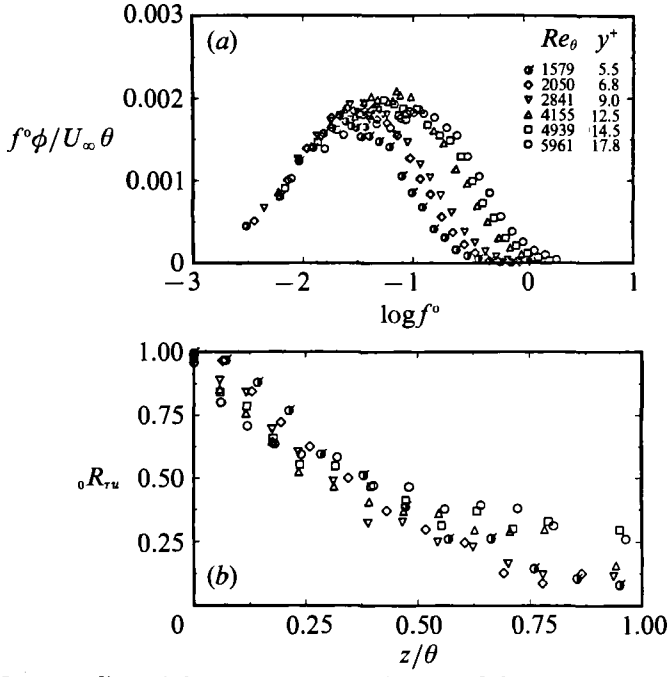

FIGURE 6. (*a*) Outer scaling of the power spectral density of the streamwise velocity fluctuations in the buffer region ($y/\theta = 0.078$), and (*b*) outer scaling characteristics of the spanwise correlation coefficient at $y/\theta = 0.078$, matching $f^o = f\theta/U_\infty$ for filter 0. Symbols in (*b*) as in (*a*).

$f^o = f\theta/U_\infty \leqslant 0.01$, corresponding to 8–23 Hz for $Re_\theta = 1579$–5961), an excellent collapse of the data in figure 6(*a*) is obtained. Thus, it appears that the appropriate cutoff frequency for the outer-scaled structures is less than or equal to 8 Hz for $Re_\theta = 1579$, and 23 Hz for $Re_\theta = 5961$, whereas the cutoff frequency used for filter 0 is $f^+ = f\nu/u_\tau^2 = 0.0025$ (or 6–46 Hz for $Re_\theta = 1579$–5961).

Figure 6(*b*) shows $R_{ru}(z/\theta)$ for a set of filters which were designed to have the same non-dimensional cutoff frequency, $f^o = 0.008$ (this corresponds to $f \approx 6$–18 Hz for $Re_\theta = 1579$–5961). Compared to the results in figure 5, the data in figure 6(*b*) show a slight improvement in data collapse for small spanwise offsets; however, some sensitivity to Reynolds number is still observed. It is, however, interesting to note

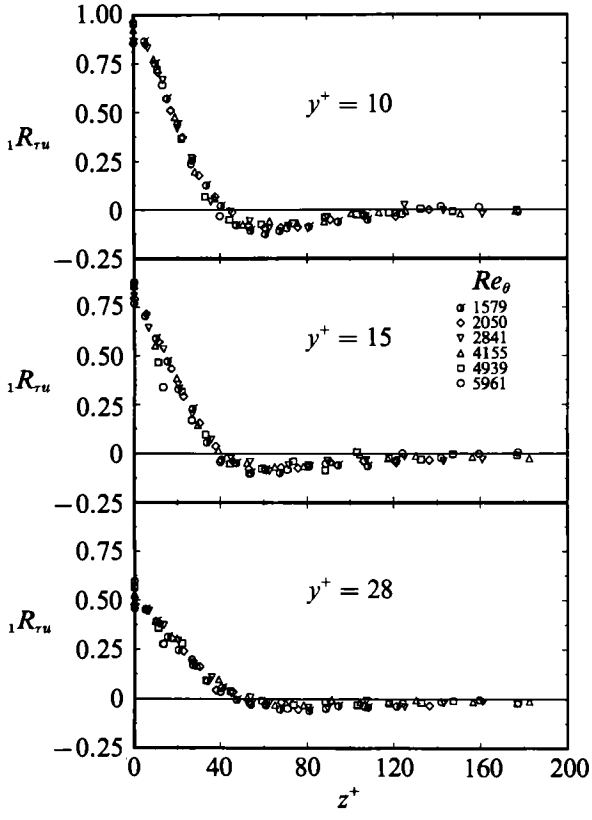

FIGURE 7. Inner scaling characteristics of the correlation coefficient in the buffer region ($y^+ = 10$, 15 and 28) for the filtered time series, using filter 1.

that the sensitivity of ${}_0R_{ru}(z/\theta)$ to Reynolds number shows two opposite trends at small and large z/θ values. For small z/θ values, ${}_0R_{ru}(z/\theta)$ decreases with Reynolds number, whereas for large z/θ values, ${}_0R_{ru}(z/\theta)$ seems to increase in a step fashion as the Reynolds number is increased from the lowest three Reynolds numbers to the highest three Reynolds numbers.

One possible explanation for the relative lack of scaling for filter 0 is the contamination received from other parts of the turbulence spectrum. To clarify, consider the correspondence between the one-dimensional and three-dimensional spectra. Since the one-dimensional k_1 spectrum results from an integration over all values of k_2 and k_3, there is contamination of the low-wavenumber spectrum by structures with high k_2 and k_3 wavenumbers. This contamination results in structures with a higher wavenumber magnitude aliasing the lower-wavenumber range in the one-dimensional k_1 spectrum. On the other hand, the high k_1 wavenumber spectra did not suffer significantly from this aliasing effect since the power spectral density at high wavenumbers is much less than at lower wavenumbers (see Bradshaw 1971, p. 40). Since the frequency spectrum is inherently one-dimensional, as in the k_1 spectrum, contamination of the low-frequency part of the spectrum by higher-frequency three-dimensional structures, which scale with inner variables, is plausible. The scaling of higher-frequency structures with wall variables (evidence of which is provided below by the results for filters 1 and 2) suggests that the aliasing of the high-frequency spectrum by even higher-frequency structures does

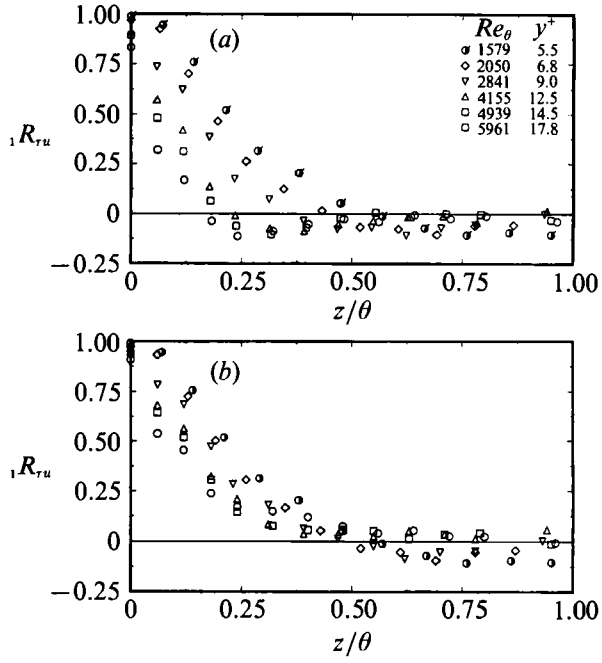

FIGURE 8. Outer scaling characteristics of the correlation coefficient in the buffer region ($y/\theta = 0.078$) for the filtered time series, matching (*a*) $f^+ = f\nu/u_\tau^2$ and (*b*) $f^o = f\theta/U_\infty$ for filter 1. Symbols in (*b*) as in (*a*).

not alter the scaling conclusions. Indeed, the correlation results pertaining to filters 3–10 (not shown here), although dynamically insignificant, scale with the inner lengthscale.

The Reynolds-number sensitivity of ${}_0R_{ru}(z/\theta)$ at large spanwise offsets is more likely to be attributable to low-Reynolds-number effects. For the range of Reynolds numbers investigated ($1579 \leqslant Re_\theta \leqslant 5961$), the outer layer does not reach equilibrium in the sense of Coles (1962) (where Re_θ has to be larger than 6000). The minimum Reynolds number for the outer-scaled correlations to collapse (if outer scaling holds) is, perhaps, not as stringent as Cole's limit, since McLean (1990) showed that his conventional correlation results collapsed when scaled with outer variables for $Re_\theta > 3000$. Close inspection of the results in figure 6(*b*) at large z/θ values reveals a good collapse (with a certain degree of scatter which is probably due to a smaller sample size for the largest scales in the low-frequency range) for the highest three Reynolds numbers ($Re_\theta > 3000$). Furthermore, this minimum Reynolds number for the collapse of the correlations seems to depend on whether the turbulent quantity scales on inner or outer variables: the results for filters 1 and higher (discussed below) show no Re_θ dependence, even for $Re_\theta = 1579$.

Figures 7–10 represent $R_{ru}(z)$ results in the buffer layer when using filters 1 and 2. An excellent collapse of ${}_1R_{ru}(z)$ and ${}_2R_{ru}(z)$ values is obtained at $y^+ = 10$, 15 and 28 (with the exception of some data scatter at $y^+ = 15$ and 28 for filter 2) when z is normalized with the inner lengthscale, see figures 7 and 9. Furthermore, at $y^+ = 10$ the prominent negative correlation peak is depicted, from figure 7, at $z^+ = 50$, and from figure 9 at $z^+ \approx 35$–40, where the negative correlation peak reaches a magnitude of about 0.25: these spanwise locations match the values for one-half the average and the most probable wavelengths of the low-speed streaks ($\lambda^+ = 100$ and 75

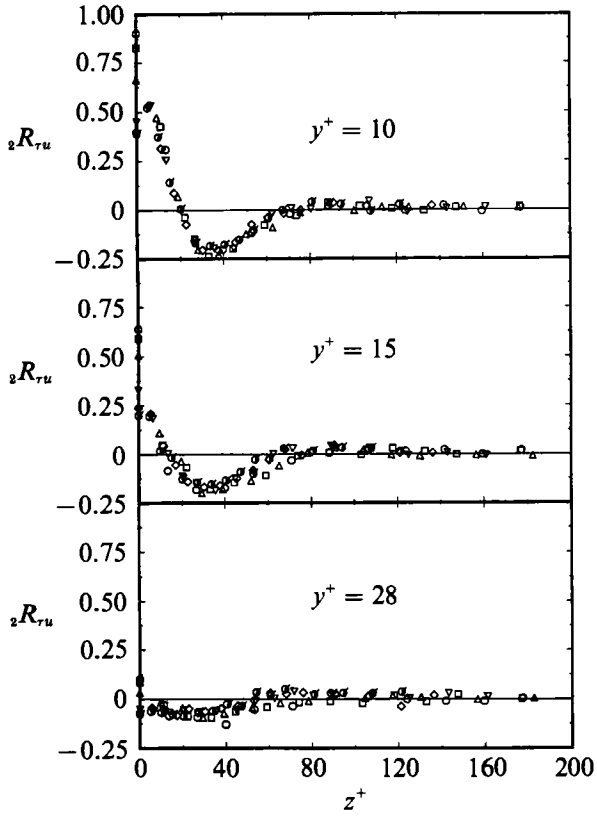

FIGURE 9. Inner scaling characteristics of the correlation coefficient in the buffer region ($y^+ = 10$, 15 and 28) for the filtered time-series, using filter 2. Symbols as in figure 7.

respectively) as found in the visual investigation of Smith & Metzler (1983). Another interesting feature of the results in figures 7 and 9 is that the structures in the frequency band allowed by filter 2 produce the maximum value for the negative correlation peak. Figures 8(*a*) and 10(*a*) demonstrate that the outer lengthscale fails to collapse $_1R_{ru}(z)$ and $_2R_{ru}(z)$ values in the frequency band allowed by filters 1 and 2; for example, as Reynolds number increases, the negative correlation peak shifts to lower z/θ locations. For the results shown in figures 8(*b*) and 10(*b*), a set of filters corresponding to filters 1 and 2 (i.e. covering a similar frequency range) but with cutoff frequencies which scale on outer variables, were used. It is clear from the results that although the scaling is better compared with matching f^+ for the cutoff frequencies, the degree of collapse is significantly worse than when scaled with wall-layer variables.

The interesting results of figures 7 and 9, in relation to the low-speed streaks, may be linked to an earlier study by Gupta, Laufer & Kaplan (1971), who recognized that the quasi-periodic structure of the near-wall region could not be depicted in the conventional long-time correlations. Using short-time correlations (VITA technique), they were able to extract instantaneous periodic signatures; however, they could not arrive at a stationary form of the correlation function that they could use to define a statistically meaningful wavelength. Instead, they used statistical techniques to extract the distribution of wavelengths from the short-time correlations, which they later used to determine an average wavelength of $\lambda^+ \approx 100$.

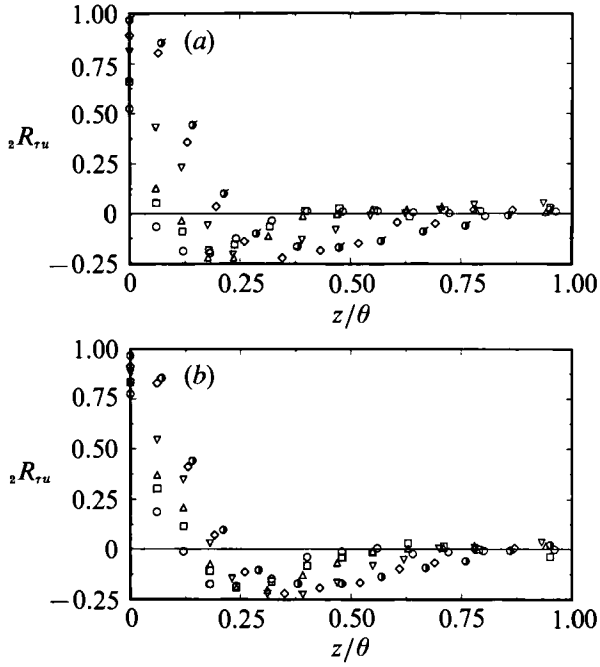

FIGURE 10. Outer scaling characteristics of the correlation coefficient in the buffer region ($y/\theta = 0.078$) for the filtered time series, matching (*a*) $f^+ = f\nu/u_\tau^2$ and (*b*) $f^o = f\theta/U_\infty$ for filter 2. Symbols as in figure 8.

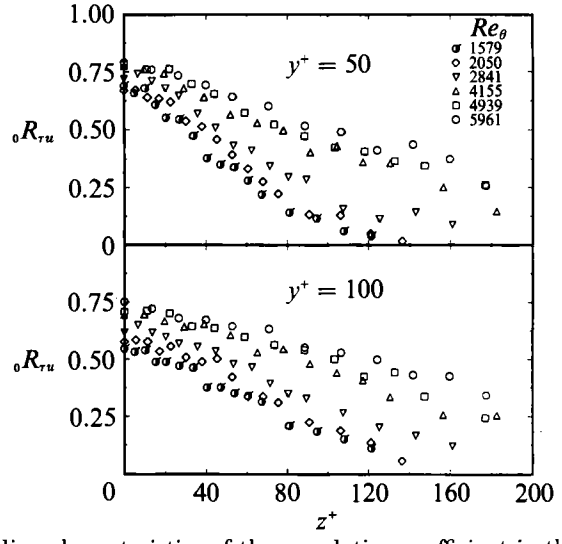

FIGURE 11. Inner scaling characteristics of the correlation coefficient in the logarithmic region ($y^+ = 50$ and 100) for the filtered time series, using filter 0.

Figures 11–16 extend the $R_{\tau u}(z)$ results to the logarithmic region. The correlation coefficient due to the low-frequency component, $_0R_{\tau u}(z)$, experiences a definite Reynolds-number effect when z is scaled using the inner lengthscale (figure 11: $y^+ = 50$ and 100), while a good collapse is obtained when z is normalized by the outer

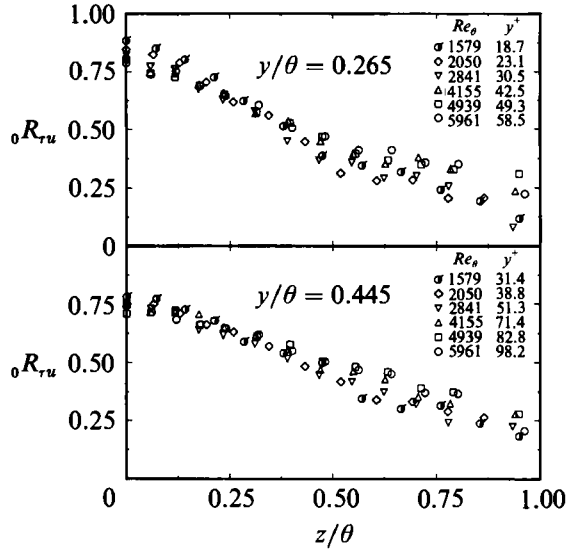

FIGURE 12. Outer scaling characteristics of the correlation coefficient in the logarithmic region ($y/\theta = 0.265$ and 0.445) for the filtered time-series, using filter 0.

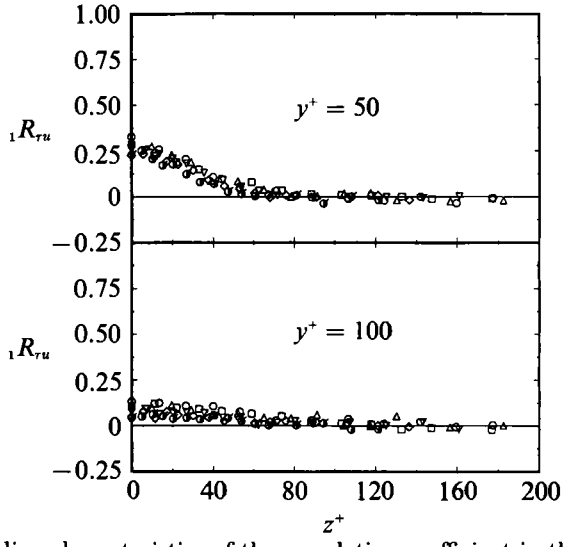

FIGURE 13. Inner scaling characteristics of the correlation coefficient in the logarithmic region ($y^+ = 50$ and 100) for the filtered time series, using filter 1. Symbols as in figure 11.

lengthscale (figure 12: $y/\theta = 0.265$ and 0.445). Moreover, when comparing the results of figure 5 ($y/\theta = 0.078$) and figure 12 ($y/\theta = 0.265$ and 0.445), it is seen that $_0R_{ru}(z/\theta)$ collapses better as y/θ increases. This agrees with one's expectation that outer-layer structures become increasingly dominant as one moves away from the wall.

Similar to the buffer layer, the results for filter 1, shown in figures 13 and 14, indicate that the inner lengthscale collapses $_1R_{ru}(z)$ better than the outer lengthscale in the lower logarithmic region. The correlation coefficient values for filter 2 are approximately zero (see figures 15 and 16) which suggests that the structures in this frequency band do not contribute significantly to $R_{ru}(z)$ in the logarithmic region.

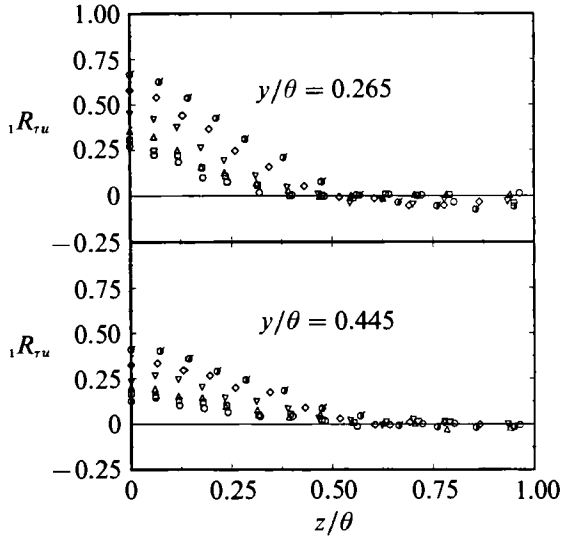

FIGURE 14. Outer scaling characteristics of the correlation coefficient in the logarithmic region ($y/\theta = 0.265$ and 0.445) for the filtered time series, using filter 1. Symbols as in figure 12.

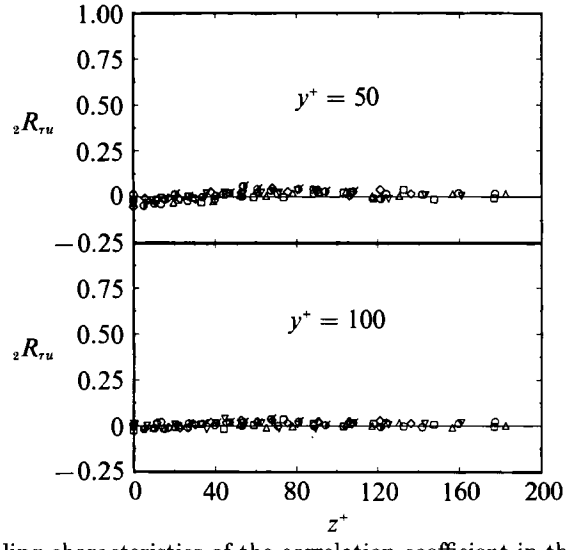

FIGURE 15. Inner scaling characteristics of the correlation coefficient in the logarithmic region ($y^+ = 50$ and 100) for the filtered time series, using filter 2. Symbols as in figure 11.

3.2. *Choice of cutoff frequencies*

Two important questions which directly impact the results presented above are, first, how much lower in value can f^+ for the cutoff frequency of filter 1 be, and still produce excellent collapse with wall variables (figures 7 and 9) and, secondly, when choosing the cutoff frequencies for different filters, should they be scaled on inner or outer variables?

To answer the first question, five band-pass filters were designed to span the narrow frequency band which extends from zero to the lower cutoff frequency of filter 1. The power spectra of the turbulent signal after filtering with these five filters

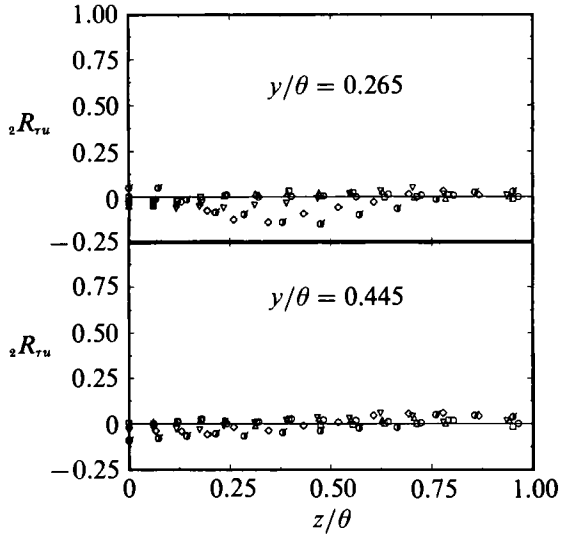

FIGURE 16. Outer scaling characteristics of the correlation coefficient in the logarithmic region ($y/\theta = 0.265$ and 0.445) for the filtered time series, using filter 1. Symbols as in figure 12.

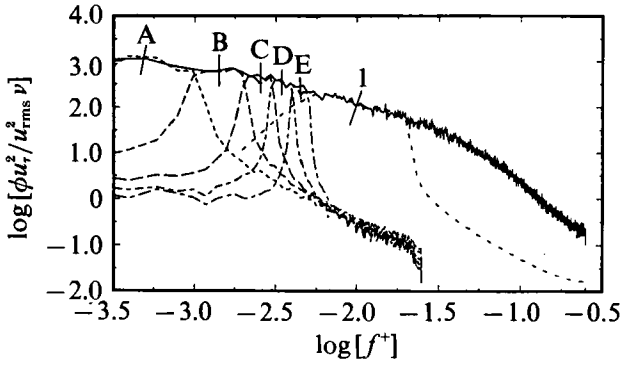

FIGURE 17. Power spectral density of the unfiltered (solid line) and filtered turbulent signal (for filters A, B, C, D, E and 1) plotted on log-log coordinates.

(labelled A, B, C, D and E) are plotted in figure 17 along with the power spectra when filtered using filter 1 and the unfiltered turbulent signal. As the frequency range increases from the lowest frequency (filter A) to the highest frequency (filter E), the spanwise extent for which wall scaling collapses $R_{\tau u}(z^+)$, gradually increases from $z^+ \approx 10$ to $z^+ \approx 60$, as seen from figure 18 for filters A, C and E. However, wall scaling is not observed for the entire range of spanwise offsets for filters A–E. It is also interesting to note that the existence of a wall-scaled region, albeit small, for filters A–C may explain the sensitivity of ${}_0R_{\tau u}(z/\theta)$ to Re_θ at small spanwise offsets (figures 5 and 6*b*). That is, although outer-layer effects appear unimportant beyond $f^+ \approx 0.0025$ (cutoff frequency of filter 1), wall-layer structures seem to have a measurable effect on the correlation coefficient in the low-frequency range with this effect getting weaker for lower frequency values.

Moving on to the second question, the correlation results at $y^+ = 10$, obtained for a set of filters corresponding to filters 1 and 2, but with cutoff frequencies which scale

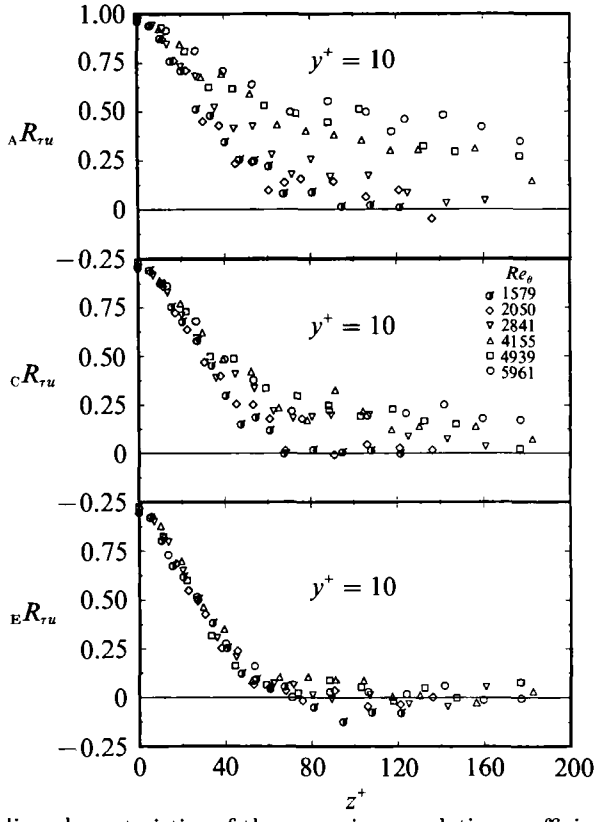

FIGURE 18. Inner scaling characteristics of the spanwise correlation coefficient results at $y^+ = 10$ for the filtered time series, using filters A, C and E.

on outer variables, are presented in figures 19(*a*) and 19(*b*) respectively. Comparing figure 19 to figures 7 and 9, it is evident that wall scaling is attained only when the cutoff frequencies of the filters are scaled on wall variables. Alternatively, comparing figure 5 to figure 6(*b*), one does not observe a significant difference in the data collapse with outer variables when choosing the cutoff frequency of the low-pass filter to scale on wall or outer variables. Thus, it seems appropriate to choose a high-pass filter with a cutoff frequency of $f^+ \approx 0.0025$ to account for the majority of the wall-layer turbulent motions, and a low-pass filter with a cutoff frequency smaller than $f^+ \approx 0.0025$ to isolate turbulent motions dominated by outer-layer structures.

4. Discussion

The results presented above may be used to explain the lack of wall scaling of the conventional correlation coefficients, $R_{uu}(z)$ and $R_{ru}(z)$, in the near-wall region as found in the results by McLean (1990) and Wark *et al.* (1991). The results from figure 4 indicate that the low-frequency structures give rise to a correlation coefficient that increases monotonically with increasing Reynolds number when scaled with wall variables. Since the spanwise correlation coefficient, $R_{ru}(z)$, due to structures that *occupy* the remainder of the spectrum (i.e. filters 1–10) scales on the inner lengthscale (see figures 7–10), one can conclude that the low-frequency structures are responsible for the lack of wall scaling of $R_{ru}(z)$. Furthermore, the positive values of $_0R_{ru}(z^+)$ when

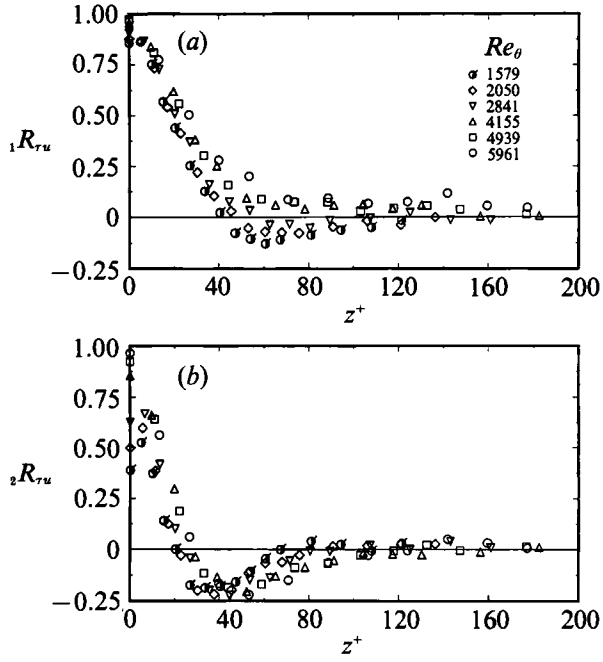

FIGURE 19. Inner scaling characteristics of the spanwise correlation coefficient results at $y^+ = 10$, for the filtered time series; matching $f^\circ = f\theta/U_\infty$ for (*a*) filter 1 and (*b*) filter 2. Symbols in (*b*) as in (*a*).

added to the negative values of $_1R_{ru}(z)$ and $_2R_{ru}(z)$ (with appropriate weighting factors) result in a positive correlation coefficient, thus obscuring the prominent negative peak of the correlation curves.

Based on the findings of the current investigation, one can reasonably assume that the contribution of the outer-layer structures to the streamwise velocity fluctuations in the near-wall region are confined within the frequency band of filter 0, whereas the rest of the u-spectrum is occupied by turbulent motions that scale on the viscous lengthscale. This raises the question of which of these two types of motions is more important in the dynamics of the wall layer. The percentage contribution to the total streamwise fluctuations energy ($\overline{u^2}$) in the near-wall region, due to outer-layer structures (filter 0) and energetic wall-layer eddies (filters 1 and 2), is plotted in figure 20 for five different y^+ positions. The energy in the higher-frequency structures accounts for only 1 to 2% of the total u-fluctuations and is not included in figure 20. At low Reynolds numbers most of the u-energy is contained in wall-layer eddies; however, as Reynolds number increases, the contribution from the outer-layer structures to $\overline{u^2}$ increases and exceeds the contribution from wall-layer eddies. A very pertinent question at this point is whether wall-layer eddies are significant at all at high Reynolds numbers of practical interest.

The results of figure 20 should, however, be viewed with caution. As Bradshaw (1967) pointed out, the successful scaling of turbulent eddies with wall variables implies that these eddies are responsible for producing the turbulent shear stress in the near-wall layer. The information obtained from figure 20 indicates that the energy of outer-layer structures increases with Reynolds number, but it does not shed light on the relative role of outer- and inner-layer structures in relation to the process of Reynolds-stress production. This was investigated further using a set of

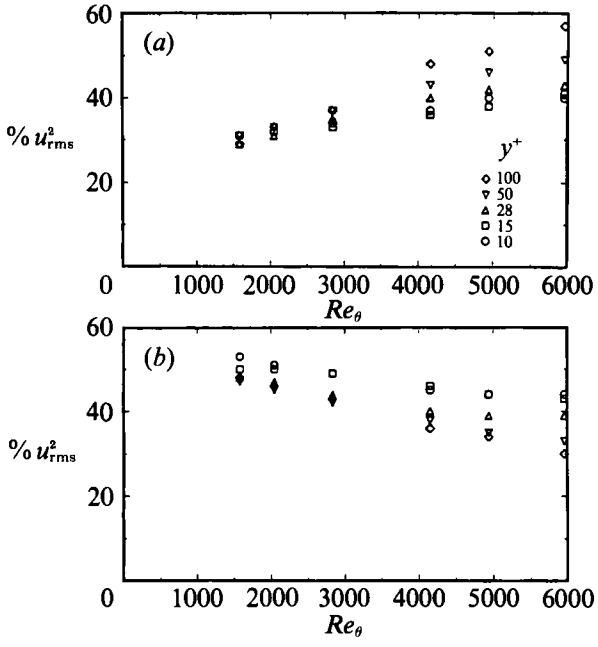

FIGURE 20. Comparison between the contribution of (*a*) outer-layer structures (filter 0) and (*b*) energetic wall-layer events (filters 1 and 2) to the energy in the streamwise velocity fluctuation at different heights in the boundary layer, for $1579 \leqslant Re_\theta \leqslant 5961$. Symbols in (*b*) as in (*a*).

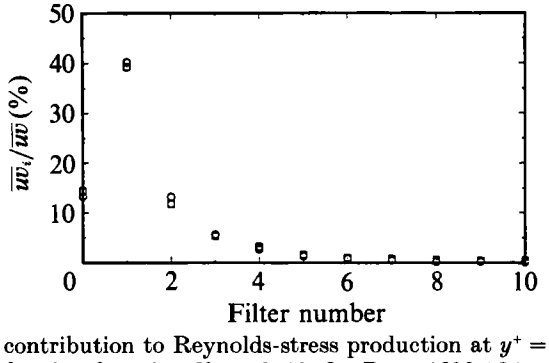

FIGURE 21. Relative contribution to Reynolds-stress production at $y^+ = 35$ due to band-pass filtered u- and v-signals, using filters 0–10, for $Re_\theta = 1600$ (○) and 4600 (□).

simultaneous u and v measurements taken using an $\times$-wire probe positioned in the boundary layer at $y^+ = 35$ for $Re_\theta = 1600$ and 4600. Both u- and v-signals were filtered using the 11 filters described in this paper, and the Reynolds stress ($\overline{uv}$) was subsequently calculated for each frequency band. The percentage of the total Reynolds stress produced by turbulent motions within the individual frequency bands of the different filters is plotted in figure 21 for the two different Reynolds numbers. Notice that the sum of the results in figure 21 is about 82% (instead of 100%) since certain frequency bands in the turbulent spectrum were not passed by any of the filters (see figure 1). The results indicate that, independent of Reynolds number, the Reynolds-stress production is dominated by wall-layer eddies which produce about 75–80% of the total Reynolds stress with the eddies in the frequency

band of filter 1 contributing most to the production process. The authors are aware of the fact that the ×-wire data may be affected by sensor averaging effects; however, if anything, a better probe resolution is expected to increase the contribution of higher-frequency wall eddies to $\overline{uv}$ production.

Since $R_{\tau u}(z^+)$ due to turbulent motions with frequencies allowed by filter 1 produce the negative correlation peak (see figure 7) commonly associated with the low-speed streaks, the results from figure 21 suggest that these streaks, and related turbulent motions, are responsible for most of the Reynolds-stress production in the near-wall region. The breakup of low-speed streaks into violent turbulent motions leading to a considerable amount of Reynolds-stress production has been known since the early work of Kim, Kline & Reynolds (1971). Furthermore, the dominant role of wall-layer structures in the production of Reynolds stress in the near-wall region agrees with the wall scaling of the frequency of occurrence of Reynolds-stress-producing events (a generally, but not exclusively, accepted result). Evidence of wall scaling of the frequency of occurrence of Reynolds-stress-producing events can be found in the work by Blackwelder & Haritonidis (1983) and Luchik & Tiedermann (1986), amongst others.

The above results provide strong support for Townsend's hypotheses of 'active' and 'inactive' motions which views the turbulent motion in the wall layer to be composed of two parts: (i) an 'active' wall-layer turbulent motion which is responsible for the production of the turbulent shear stress and, hence, its statistical properties scale on wall variables; and (ii) a large-scale 'inactive' motion which neither interacts with the wall-layer eddies (due to the disparity in lengthscales between inner- and outer-layer structures) nor contributes to the turbulent shear stress. The 'active' and 'inactive' motions theory was explored by Bradshaw (1967), who used frequency spectra measured in zero- and adverse-pressure-gradient boundary layers. The universality of the spectra when scaled on τ and y in boundary layers with outer motions of varying strength (higher adverse pressure gradients correspond to stronger outer motions), implied that the outer motions were 'inactive' within the wall layer. More recent support of Townsend's hypotheses was also given by Beljaars, Krishna Prasad & de Vries (1981) using results from a proposed structural model, and the correlation results in zero- and adverse-pressure-gradient boundary layers of McLean (1990).

5. Conclusions

Band-pass filters were used to investigate the relative contribution of outer-layer and wall-layer structures to the spanwise correlation coefficient $R_{\tau u}(z)$. Structures contributing to the low-frequency range ($f^o = f\theta/U_\infty \leqslant 0.008$) were found to be responsible for the lack of scaling of $R_{\tau u}(z^+)$ and for the disappearance of the 'negative dip' (often associated with low-speed streaks) of the spanwise correlation. This signature of the low-speed streaks was found to exist in the intermediate frequency range for all Re_θ investigated and was shown to exhibit wall-layer scaling.

Investigating the relative role of the individual structures in the dynamics of the near-wall region, it was found that the contribution of the outer-layer structures to the streamwise velocity fluctuations increases with increasing Reynolds number. Nevertheless, the Reynolds-stress production was found to be dominated by wall-layer structures and the role of outer-layer structures in the production process is, almost, 'inactive' as speculated by Townsend in his hypothesis of 'active' and 'inactive' motions.

The authors sincerely acknowledge the support for the current investigation by the Air Force Office of Scientific Research (AFOSR-90-0171), monitored by Dr J. McMichael.

REFERENCES

ALFREDSSON, P. H., JOHANSSON, A. V., HARITONIDIS, J. H. & ECKELMANN, H. 1988 *Phys. Fluids* **31**, 1026.

BELJAARS, A. C. M., KRISHNA PRASAD, K. & VRIES, D. A. DE 1981 *J. Fluid Mech.* **112**, 33.

BLACKWELDER, R. F. & HARITONIDIS, J. H. 1983 *J. Fluid Mech.* **132**, 87.

BRADSHAW, P. 1967 *J. Fluid Mech.* **30**, 241.

BRADSHAW, P. 1971 *An Introduction to Turbulence and its Measurement.* Pergamon.

BROWN, G. L. & THOMAS, S. W. 1977 *Phys. Fluids* **20**, 243.

CHEN, C. H. P. & BLACKWELDER, R. F. 1987 *J. Fluid Mech.* **89**, 1.

CLAUSER, F. H. 1956 *Adv. Appl. Mech.* **4**, 1, 51.

COLES, D. E. 1962 *Rand Rep. R*-403-*PR.*

GUPTA, A. K., LAUFER, J. & KAPLAN, R. E. 1971 *J. Fluid Mech.* **50**, 493.

KIM, H. T., KLINE, S. J. & REYNOLDS, W. C. 1971 *J. Fluid Mech.* **50**, 133.

KREPLIN, H. P. & ECKELMANN, H. 1979 *J. Fluid Mech.* **95**, 305.

LAUFER, J. 1950 *NACA Tech. Note* TN2123.

LUCHIK, T. S. & TIEDERMANN, W. G. 1986 *J. Fluid Mech.* **174**, 481.

MCCLELLAN, J. H., PARKS, T. W. & RABINER, L. R. 1979 *Programs for Digital Signal Processing* (ed. Digital Signal Processing Committee, IEE Acoustics, Speech and Signal Processing). IEEE Press.

MCLEAN, I. R. 1990 The near wall eddy structure in an equilibrium turbulent boundary layer. Ph.D. thesis, University of Southern California.

ROBINSON, S. K. 1991*a* *NASA Tech. Mem.* 103859.

ROBINSON, S. K. 1991*b* *Ann. Rev. Fluid Mech.* **24**, 601.

SMITH, C. R. & METZLER, S. P. 1983 *J. Fluid Mech.* **129**, 27.

SPALART, P. R. 1988 *J. Fluid Mech.* **187**, 61.

TOWNSEND, A. A. 1961 *J. Fluid Mech.* **11**, 97.

WARK, C. E. & NAGIB, H. M. 1991 *J. Fluid Mech.* **230**, 183.

WARK, C. E., ROBINSON, S. K. & NAGUIB, A. M. 1991 *AIAA 29th Aerospace Sciences Meeting, Reno, Nevada; Paper AIAA* 91-2035.

WEI, T. & WILLMARTH, W. W. 1989 *J. Fluid Mech.* **204**, 57.